ChemPhotoChem

Research Article
doi.org/10.1002/cptc.202300073

Chemistry Europe
European Chemical Societies Publishing

www.chemphotochem.org

Special Collection

Triplet Formation and Triplet-Triplet Annihilation Upconversion in Iodine Substituted Non-Orthogonal BODIPY-Perylene Dyads

Keshav Kumar Jha[+],[a, b] Amrutha Prabhakaran[+],[c] Rengel Cane Sia,[d] Ruben Arturo Arellano Reyes,[c] Nirod Kumar Sarangi,[c] Tingxiang Yang,[a, b] Krishan Kumar,[a] Stephan Kupfer,[b] Julien Guthmuller,[d] Tia E. Keyes,[c] and Benjamin Dietzek-Ivanšić*[b]

BODIPY-perylene dyads have emerged as useful metal free sensitizers for triplet-triplet annihilation upconversion (TTAUC), these dyads are capable of efficient triplet generation *via* spin-orbit charge transfer intersystem crossing (SOCT-ISC). This important route to triplet formation requires dyads in which two moieties are oriented perpendicular to each other. In this contribution, we give a deeper insight on the behavior of recently reported BODIPY-perylene dyads, where BODIPY-perylene dihedral exhibits a non-orthogonal dyad geometry. The intersystem crossing of BODIPY-perylene dyads with and without iodine are investigated using femtosecond transient absorption (fs-TA) and nanosecond transient absorption (ns-TA) spectroscopy. The concurrent decay of the singlet charge transfer state (^{1}CT) and rise of triplet states in both the iodinated and non-iodinated dyads confirms the SOCT-ISC as the main intersystem crossing pathway despite the altered geometry of the dyads. The presence of an iodine atom on the BODIPY-moiety enables intersystem crossing 2.6-times faster and provides a higher triplet yield with respect to dyad without iodine. The upconversion quantum yield (ϕ_S^{UC}) is 8.4-times higher in the sample containing iodinated dyad as sensitizer and perylene as annihilator. The triplet-triplet energy transfer rate (k_{TTET}) is ~8×10^8 $M^{-1}s^{-1}$ for both iodinated and non-iodinated sensitizer containing TTAUC systems in 1,4-dioxane.

Introduction

The 4,4-difluoro-4-bora-3a,4a-diaza-s-indacene (BODIPY) fluorophore and its derivatives have attracted a lot of attention due to their high extinction coefficient and tunable photophysical properties.[1–4] It has found applications in biological imaging,[5,6] photodynamic therapy,[7,8] photocatalysis,[8] dye-sensitized solar cells[8,9] and triplet-triplet annihilation upconversion (TTAUC).[10] The BODIPY chromophore fosters very high fluorescence quantum yields but low triplet yields,[1,4] which limits its application in a number of processes including photodynamic therapy and TTAUC.[2,4,8,11] The triplet yield can be promoted in BODIPY molecules by introducing heavy atoms such as iodine or bromine substituents.[3,12,13] The substitution of iodine offers higher efficiency than the incorporation of bromine atom.[14] The heavy atom enhances spin orbit (SO) coupling of S_1—T_1, therefore enhancing the intersystem crossing efficiency by the heavy atom effect.

The excited triplet formation in donor-acceptor dyads can be facilitated by spin-orbit charge transfer intersystem crossing (SOCT-ISC).[2] Molecular donor-acceptor dyads with BODIPY as an acceptor have been synthesized, *e.g.*, with pyrene, anthracene and perylene as donors.[2,4,11,15–24] The triplet lifetime of the species formed by charge recombination in a BODIPY-perylene dyad has been determined to be 436 μs which is much higher than the triplet lifetime of 62 μs of the 2,6-iodo BODIPY derivative, *i.e.*, without charge transfer and recombination.[15] For efficient SOCT-ISC, molecular donor-acceptor configurations need to be nearly orthogonal.[24] Therefore, typically the donor moiety is linked to the meso-position of the acceptor-moiety making the donor-acceptor configuration nearly orthogonal.[25] However, we have recently reported efficient TTAUC using BODIPY-perylene dyad, where perylene is

[a] K. Kumar Jha,[+] T. Yang, Dr. K. Kumar
Research Department Functional Interfaces, Leibniz Institute of Photonic Technology Jena, Jena 07745, Germany

[b] K. Kumar Jha,[+] T. Yang, Dr. S. Kupfer, Prof. Dr. B. Dietzek-Ivanšić
Institute of Physical Chemistry and Abbe Center of Photonics, Friedrich Schiller University Jena, Jena 07743, Germany
E-mail: benjamin.dietzek@uni-jena.de

[c] A. Prabhakaran,[+] R. A. Arellano Reyes, Dr. N. Kumar Sarangi, Prof. Dr. T. E. Keyes
School of Chemical Sciences and National Centre for Sensor Research, Dublin City University, Dublin 9, Ireland

[d] R. Cane Sia, Dr. J. Guthmuller
Institute of Physics and Applied Computer Science, Faculty of Applied Physics and Mathematics, Gdańsk University of Technology, 80233 Gdańsk, Poland

[+] Equal contribution

Supporting information for this article is available on the WWW under https://doi.org/10.1002/cptc.202300073

Special Collection An invited contribution to a Special Collection on Ultrafast Spectroscopy

linked to the 2-position of the BODIPY-moiety (see Scheme 1), *i.e.* leading to a non-orthogonal configuration.[26,27] In this TTAUC experiment, additional perylene in solution served as the annihilator in the overall upconversion process. In this contribution, we investigate, in detail, the photophysical processes behind the TTAUC (charge separation, charge recombination, triplet formation and energy transfer) and the effect of iodination (B2P *vs.* B2PI, see Scheme 1) on the ISC for the BODIPY-perylene dyad using computational simulations, femtosecond and nanosecond transient absorption spectroscopy.

TTAUC is a bimolecular diffusion-controlled process, initiated by the absorption of a low energy (red-NIR) photon by a sensitizer (or donor) molecule. Upon absorption, the molecule transitions to its first singlet excited state (^{1}S*), followed by intersystem crossing (ISC) to reach its first triplet excited state (^{3}S*). The triplet sensitizer molecule transfers its energy by triplet-triplet energy transfer (TTET) to a nearby annihilator (or acceptor) molecule, leading the ground state annihilator (^{1}A) to achieve its first triplet excited state (^{3}A*). Two of such triplet annihilator molecules annihilate (triplet-triplet annihilation – TTA) yielding one molecule in its first singlet excited state (^{1}A*), which is at higher energy than the ^{1}S* state. Consequently, fluorescence of ^{1}A* emits photons of higher energy than the initially absorbed photons.[28–31] The TTAUC mechanism is schematically depicted in Figure 1. In case of a dyad molecule as a sensitizer, first charge separation takes place followed by charge recombination to form a triplet of the sensitizer, the consequent processes are same as explained above.[16,32]

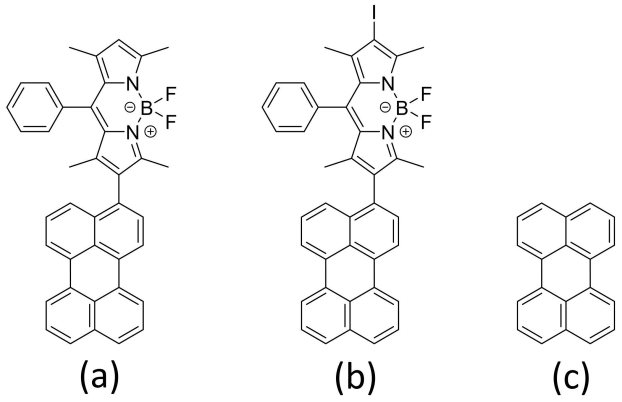

Scheme 1. (a) BODIPY-perylene dyad without iodine- B2P (b) BODIPY-perylene dyad with iodine- B2PI (c) perylene.

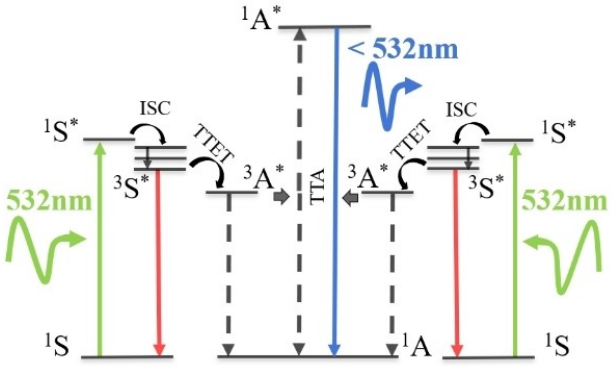

Figure 1. Schematic illustration of TTAUC mechanism. Upward green arrow depicts absorption. The downward red arrow from ^{3}S* depicts phosphorescence. The dashed line from ^{3}A* shows non-radiative decay. The bidirectional dashed arrow depicts TTA. The downward blue arrow depicts upconversion fluorescence.

Experimental Methods

Samples

B2P and B2PI synthesis protocol and characterization of compounds have been reported earlier.[26] All spectroscopic experiments are carried out in deoxygenated 1,4-dioxane, obtained from Sigma Aldrich. The samples (solution mixture of sensitizer and annihilator) are placed in 1 cm inert cuvettes to maintain the inert conditions for all the steady state and nanosecond time-resolved measurements, 1-mm inert cuvettes were used for femtosecond time-resolved measurements. Sensitizer and annihilator of different concentrations are used for the experiments, which are listed in the Table 1.

Photophysical Steady State Studies

The absorption spectra of the samples are measured using a Jasco V780 UV/Vis/NIR spectrophotometer in a quartz cuvette with 1 cm path length. The fluorescence emission spectra are measured using a FLS980 emission spectrophotometer (Edinburg Instrument) with a Xenon lamp as a white light excitation source (ozone free 450 W). The excitation wavelength for all the emission spectra is 532 nm, emission is collected in 400–500 nm range.

Photophysical Time-Resolved Studies

Femtosecond time-resolved absorption (fs-TA) measurements were performed using a home-built setup reported earlier.[33,34] Samples were placed in 1 mm pathlength quartz-made inert cuvettes for all fs-TA measurements and absorbance for all the samples at excitation wavelength is ~0.35. The pump pulse power was ~20 μJ.

Nanosecond time-resolved absorption (ns-TA) data were acquired using a custom-built setup reported earlier.[35] The electronics and programming to record the difference absorption signal (for both fs-TA and ns-TA) are developed by Pascher Instruments (Lund, Sweden). The samples were kept in 1 cm pathlength quartz-made

Table 1. The lifetimes given are obtained using nanosecond time-resolved spectroscopy. The error margin for the lifetimes of all B2PI samples is within 10% and for all B2P samples is within 20%.

Constituent 1	Constituent 2	Solvent	τ_1 (μs)	τ_2 (μs)	τ_3 (μs)
B2PI – 1 μM	–	dioxane	60	525	1500
B2PI – 5 μM	–	dioxane	66	155	560
B2P – 5 μM	–	dioxane	80	900	2500
B2PI – 5 μM	perylene – 50 μM	dioxane	17	107	512
B2P – 5 μM	perylene – 50 μM	dioxane	18	812	2000

inert cuvettes for all ns-TA measurements. The pump pulse energy was 0.12 ± 0.01 mJ for all ns-TA measurements.

Computational Studies

The quantum chemical calculations were performed with the programs Gaussian 16[36] and Orca 5.0.[37] Density functional theory (DFT) was employed to calculate the geometry and the harmonic vibrational frequencies of the ground state (S_0), while time-dependent DFT (TDDFT) was used to compute the singlet and triplet excited states properties (*i.e.* energy, transition dipole moment, geometry, vibrational frequencies). The DFT and TDDFT calculations were done with the MN15[38] exchange-correlation (XC) functional in association with the def2-SVP basis set[39,40] for the geometry optimizations in Gaussian. The excited state energies were then re-calculated with the larger basis set def2-TZVP in Orca. Density functional dispersion corrections were included using the GD3 model[41,42] using the parameter reported in Goerigk et al.[43] for MN15. The effects of the solvent (1,4-dioxane, ε = 2.2099) were considered by the polarizable continuum model[44] (PCM) using the SMD solvation model.[45] The excited states geometries, and vibrational frequencies were calculated with the equilibrium procedure of solvation. The vibrational frequency calculations showed that all obtained geometries were minima of the potential energy surface. The optimization of the T_2 geometry was unsuccessful due to lack of convergence.

Furthermore, scalar relativistic TDDFT calculations were performed with Orca using the Douglas-Kroll-Hess (DKH) method in order to estimate the spin-orbit couplings (SOCs) between the singlet state S_1 and the triplet states T_1, T_2 and T_3. These calculations were performed by using the previously optimized geometries of the S_0, S_1, T_1 and T_3 states. The XC functional MN15 was employed together with the basis sets DKH-def2-TZVP (for the atoms H, C, N, B, F) and SARC-DKH-TZVP (for the I atom) as well as the auxiliary basis set SARC/J. The effects of the solvent (1,4-dioxane) were considered by CPCM using the SMD solvation model. The SOC between the S_1 and T_n states was calculated according to Equation (1):

$$\mathrm{SOC} = \sqrt{\sum_{m_s=0,\pm1} \left|(H_{SO})_{Tm_s,S}\right|^2} \quad (1)$$

where $(H_{SO})_{Tm_s,S} \equiv \langle \phi_{Tm_s} | H_{SO} | \phi_S \rangle$ is a matrix element of the spin-orbit Hamiltonian (H_{SO}) between the triplet electronic state ϕ_{Tm_s} and the singlet electronic state ϕ_S.

Results and Discussion

Steady State Absorption and Emission Spectroscopy

The details of absorption, fluorescence emission, fluorescence quantum yield, upconversion emission and threshold power density (I_{th}) have been reported recently,[26] a brief summary is given here before describing time-resolved data. The absorption and emission spectra of B2P, B2PI and perylene in dioxane are shown in Figure 2a and 2b, respectively. The absorption peaks of B2P and B2PI are at 517 nm and 532 nm, respectively; the bathochromic shift to the absorption spectrum of B2PI is due to incorporation of an iodine atom to the BODIPY-moiety.[46] Upon 400 nm, emission is observed at 635 nm and 655 nm for B2P and B2PI, respectively. The bathochromic shift in emission spectra is also due to iodine and has been reported before.[3,17]

The sample containing B2PI (1 μM) and perylene (10 μM) is denoted **BPI1-P10**, similarly B2P (1 μM) and perylene (10 μM) is labelled **BP1-P10** for convenience. The upconversion emission of **BPI1-P10** and **BP1-P10** where B2P, B2PI are used as sensitizer and perylene as annihilator is shown in Figure 2c. The peaks at 443 nm and 473 nm resemble the fluorescence signal of perylene (see Figure 2b). The integrated upconversion emission intensity of **BPI1-P10** is 8.7 times higher than the intensity of the **BP1-P10** sample. The upconversion quantum yield (ϕ_S^{UC}) of **BPI1-P10** and **BP1-P10** at 450 mW cm^{-2} are 22% and 2.6%, respectively; similar to the upconversion emission intensity, ϕ_S^{UC} is 8.4 times higher in the **BPI1-P10** sample (see, SI for details). The threshold power density (I_{th}) for the **BPI-P10** and **BPI1-P10** were reported to be 51 mWcm^{-2} and 126 mWcm^{-2}, respectively.[26] The higher upconversion intensity for **BPI-P10** sample was attributable to the enhanced intersystem crossing

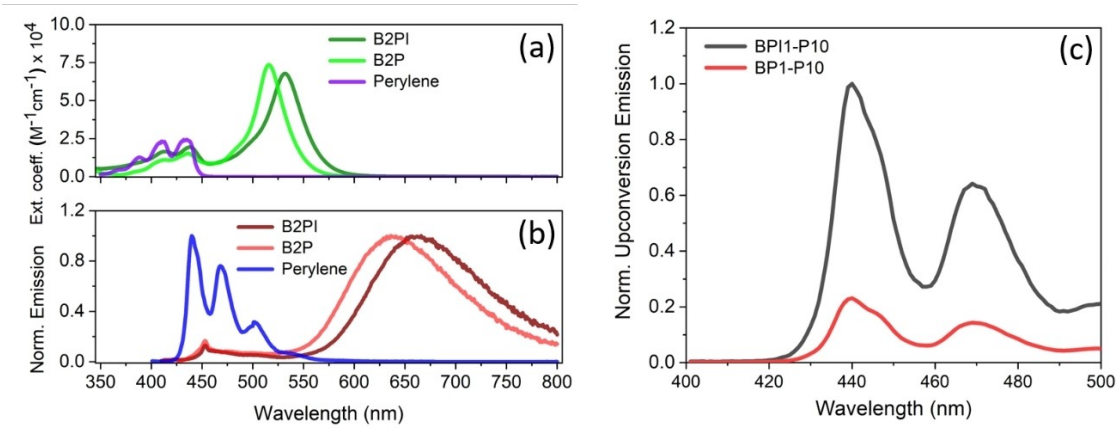

Figure 2. (a, b) Absorption and emission spectra of Ph-2-BODIPY-perylene (B2P), Ph-2-BODIPY-perylene-iodine (B2PI) and perylene in 1,4-dioxane, upon 400 nm excitation. (c) Normalized TTA-UC emission from **BPI1-P10** and **BP1-P10** in deaerated 1,4-dioxane (at 532 nm excitation), the emission spectra are normalized with respect to the maximum of emission peak (443 nm) from the **BPI1-P10** sample.

due to the presence of iodine (*vide infra*) under otherwise identical experimental conditions.[3,47–49]

Time-Resolved Absorption and Emission Spectroscopy

In order to understand the photophysical processes underlying the TTAUC, we examined the fs-TA and ns-TA of B2P and B2PI in the absence and presence of perylene to investigate the processes occurring over sub-picosecond to microsecond time-scale.

The fs-TA of B2P and B2PI are shown in Figure 3a and 3b, respectively. In both data sets negative differential absorbance from approximately 500 to 575 nm is attributed to the ground state bleach (GSB) of the BODIPY unit and negative peaks below 450 nm are attributed to the GSB of perylene unit, evident from its resemblance to absorbance shown in inverted green. In line with literature reports, we associate the positive peak at 575 nm with the absorption of the perylene-BODIPY cation-anion radical pair.[11,15,24]

The formation of GSB of both the units (BODIPY and perylene) and the subsequent appearance of positive Δabsorbance of the $BODIPY^{-\bullet}$ and $perylene^{+\bullet}$ radical pair (*ca.* 600 nm) indicates the formation of a charge-transfer state (CT). The concomitant decay of ^{1}CT ($BODIPY^{-\bullet}$ and $perylene^{+\bullet}$) absorption and the rise of ESA of triplet species reveal triplet formation by charge recombination (see kinetic traces at 480 nm and 580–600 nm, Figure 3c–d). These observations indicate the formation of triplet species by SOCT-ISC, which is in line with the previous investigation by Wang et al. using time-resolved electron paramagnetic resonance (TREPR) spectroscopy.[15] We observed three contributions to the triplet state ESA, which may arise from BODIPY-centered, perylene-centered and ^{3}CT states; where, SOCT-ISC remains the major ISC pathway (*vide supra*).

The kinetics obtained from the experiments were analyzed by global fitting with the program KiMoPack;[50] kinetics from GSB (485 nm) and absorption of ^{1}CT (580–600 nm) regions are shown in Figure 3c–d. The global analysis reveals four-time constants along with an infinite component for the B2P sample: $\tau_1 = 0.6$ ps, $\tau_2 = 5$ ps, $\tau_3 = 273$ ps, $\tau_4 = 1785$ ps and τ_{inf}; similarly, four-time constants for B2PI sample: $\tau_1 = 0.6$ ps, $\tau_2 = 4.5$ ps, $\tau_3 = 288$ ps, $\tau_4 = 662$ ps and τ_{inf}. τ_1, τ_2 and τ_3 are the same within in experimental error for each compounds, only τ_4 is significantly affected by iodination.

In B2P and B2PI the BODIPY-perylene dihedral angle is estimated to be 58° in the electronic ground state geometry (S_0), while it decreases to 41° in the first excited state (S_1),[26] see Figure 4 and 5 for details. The relaxation from the Franck-Condon geometry to the relaxed S_1 geometry takes place on a sub-picosecond timescale;[51] consequently, we associate the shortest time constant, τ_1 with the geometrical relaxation. The absorption of the ^{1}CT near 600 nm of both the molecules grows

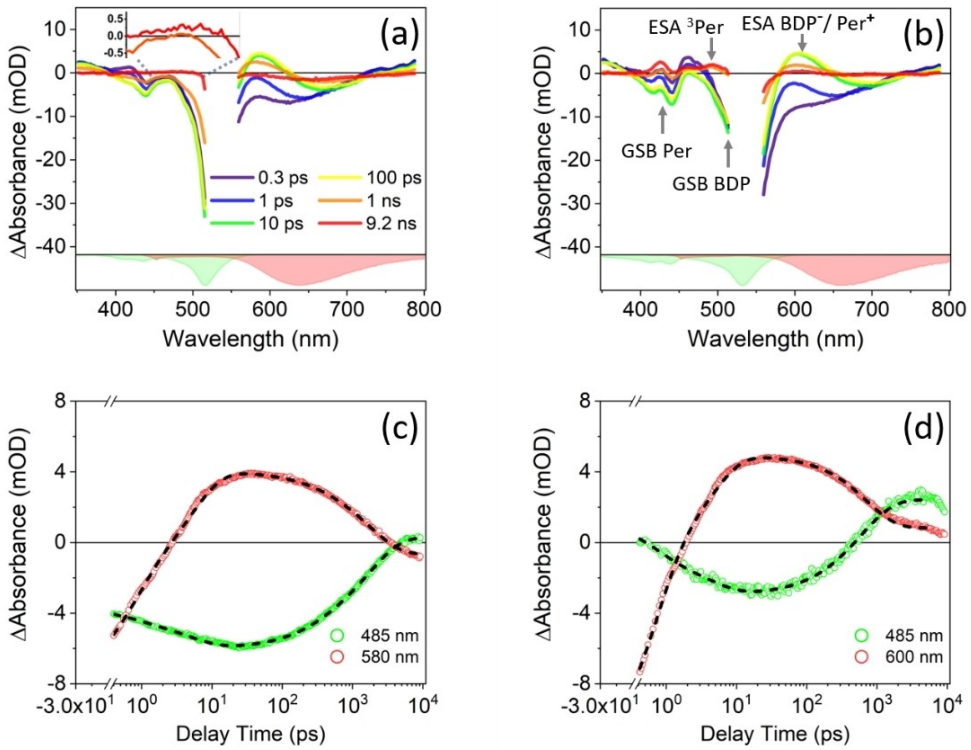

Figure 3. Femtosecond transient absorption spectra of (a) B2P and (b) B2PI; both spectra are measured in 1,4-dioxane. In the bottom- inverted absorbance is in green and inverted emission is in red of the respective samples. The excitation wavelength is 532 nm for both samples. Labels are identical for (a) and (b). Per: perylene, BDP: BODIPY. ^{3}Per: perylene-centered triplet. Kinetic traces of (c) B2P, $\tau_1 = 0.6$ ps, $\tau_2 = 5$ ps, $\tau_3 = 273$ ps, $\tau_3 = 1785$ ps and τ_{inf} – infinite component (d) B2PI, $\tau_1 = 0.6$ ps, $\tau_2 = 4.5$ ps, $\tau_3 = 288$ ps, $\tau_3 = 662$ ps and τ_{inf} – infinite component. Dashed black lines in B2P and B2PI depict fit to the respective kinetics, error margin of the time constant can be within 10% of the given value.

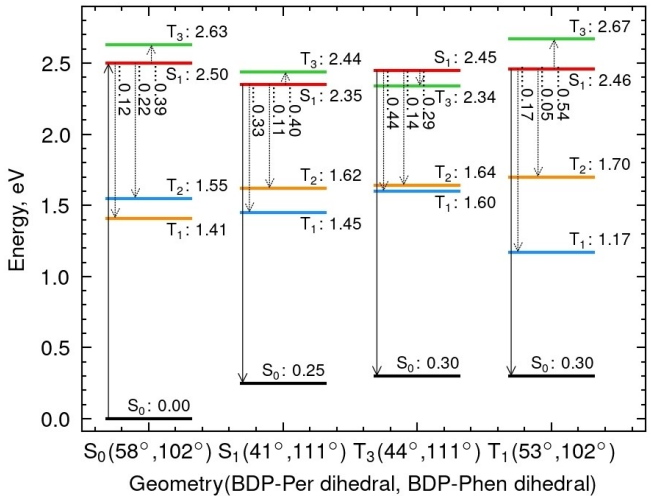

Figure 4. The energies (eV) of the states and SOCs (cm^{-1}) between the S_1 and T_n states in B2P at four different geometries. The colors indicate the main orbital character of the states: Red: ^{1}CT state, Green: ^{3}CT state, Blue: perylene-centered state, Yellow: BODIPY-centered state.

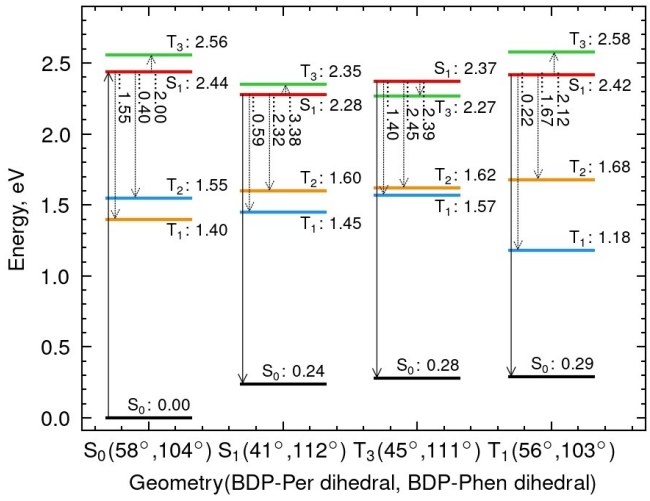

Figure 5. The energies (eV) of the states and SOCs (cm^{-1}) between the S_1 and T_n states in B2PI at four different geometries. The colors indicate the main orbital character of the states: Red: ^{1}CT state, Green: ^{3}CT state, Blue: perylene-centered state, Yellow: BODIPY-centered state.

up to *ca.* 30 ps (see Figure 3c–d), which indicates the population growth of species $BODIPY^{-\bullet}$ and $perylene^{+\bullet}$; hence, the τ_2 time-constant is assigned to build up of charge transfer state (^{1}CT),[27] these time constants match with the literature reports on BODIPY-dyads.[32]

The absorption of the radical pair at *ca.* 580–600 nm starts decaying at delay times longer than *ca.* 20 ps for both B2P and B2P1. Simultaneously, the GSB decays and a new photoinduced absorption band forms at 485 nm, which is associated with the triplet state of the molecules. The simultaneous decay of the ^{1}CT band (kinetics 580–600 nm) and rise of the triplet absorption (kinetics 485 nm) indicate the formation of (localized) triplet states by the charge recombination.[15] The kinetics at 485 nm becomes positive (i.e. GSB of radical pair turns to ESA of triplet species) at *ca.* 5 ns for the B2P; whereas, at *ca.* 1 ns for B2PI. This observation confirms faster formation of triplet in B2PI; in turn, the time constant τ_3, which shows the same value for both B2P and B2PI is most likely not associated with ISC but rather with charge recombination to ground state (CR_S). Instead ISC is associated with τ_4, which reflects the time taken to form a triplet by charge recombination (CR_T). It is apparent that the ISC is 2.6 times faster in the iodine-containing B2PI, which highlights the role of the heavy atom in ISC. The B2PI kinetics are fitted up to 5 ns only since its triplet state starts decaying beyond 5 ns but the decay time-constant (of the triplet state) cannot be observed accurately using the dynamic range available in the fs-TA experiments. However, the triplet state of B2P continues to evolve up to 9 ns, hence, in the range of accessible delay times.[2,15,24,32]

The SOCs between the S_1 (^{1}CT) state and the three lowest triplet states (T_1, T_2 and T_3) were calculated with scalar-relativistic TDDFT at the geometries of the ground state (S_0), ^{1}CT state (S_1), ^{3}CT state (T_3) and the perylene-centered state (T_1) (see Figures 4 and 5). The charge density difference for the three lowest triplet states of B2PI is shown in Figure 6. At the ^{1}CT geometry, the SOC for the BODIPY-centered state (T_2) is significantly increased in the iodinated dyad: SOC for B2P and B2PI are 0.11 cm^{-1} and 2.32 cm^{-1}, respectively; whereas the SOC for the perylene-centered state (T_1) presents a much smaller variation, i.e., B2P (0.33 cm^{-1}) *vs* B2PI (0.59 cm^{-1}). Comparable changes in SOCs are obtained at the other geometries. Therefore, the calculations corroborate that more efficient triplet formation occurs in B2PI, and that iodination favors ISC towards the BODIPY-centered state.

The SOC for the ^{3}CT state has a comparable magnitude as the SOC for the BODIPY-centered state. Moreover, the SOC for the ^{3}CT state is also increased upon iodination, *e.g.*, SOCs of

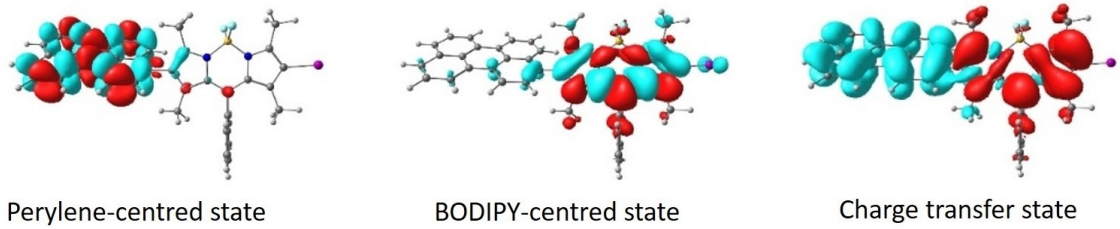

Figure 6. Iso-surfaces of charge density difference for the three lowest triplet states of B2PI. Positive (electron) and negative (hole) values are indicated in red and blue colors, respectively.

0.40 cm^{-1} and 3.38 cm^{-1} are calculated at the ^{1}CT geometry for B2P and B2PI, respectively. This indicates a possible formation of the ^{3}CT species by ISC from the ^{1}CT state. The ns-TA analysis described later in the text (see Figure 8) also confirms the presence of ^{3}CT species. The formation of BODIPY-centered triplet and perylene-centered triplet occurs through the recombination of charge by SOCT-ISC (see SI, Equation S4 and S5).[11,18] In general, the formation of the ^{3}CT state in donor-acceptor dyads can occur through radical pair intersystem crossing (RP-ISC),[52] which involves a hyperfine coupling and requires a very small singlet-triplet energy gap ($2J <$ 0.1 cm^{-1}).[52] This latter condition can be achieved by using well separated donor and acceptor moieties, which has the effect of reducing the electronic exchange interaction between the donor and acceptor, consequently leading to a small ^{1}CT-^{3}CT energy gap. The TDDFT calculations for B2P and B2PI predict a singlet-triplet energy gap larger than 70 cm^{-1} (see SI, computation section), indicating a significant coupling between the donor and acceptor. Because this energy gap is noticeably larger than 0.1 cm^{-1}, RP-ISC is unlikely to occur in these two compact dyads, in which the perylene and BODIPY moieties are only separated by a single bond.[18,52] However, due to the overlap of the donor and acceptor orbitals, a non-zero SOC is obtained between the ^{1}CT and ^{3}CT states. Therefore, it is concluded that the population of the ^{3}CT state in B2P and B2PI occurs through ^{1}CT→^{3}CT ISC induced by this SOC. A similar observation was made by Wang et al. where electron spin polarization obtained by time-resolved electron paramagnetic resonance spectroscopy (TREPR) indicated SOCT-ISC was the main intersystem crossing channel with a minor contribution of ^{3}CT was observed.[18]

Nanosecond time-resolved studies were performed on B2P, B2PI in the presence and in the absence of addition perylene in 1,4-dioxane solution to investigate the kinetics of TTAUC. The measurements were attempted with 1 μM concentration of both the molecules, as used in the steady state upconversion emission measurements, but the signal-to-noise-ratio turned out to be rather poor for the B2P containing sample (see SI, Figure S9). Consequently, a 5 μM concentration of B2P and B2PI was chosen with 50 μM perylene for the ns time-resolved upconversion studies.

Nanosecond transient absorption spectra of B2P with and without the addition of perylene are shown in Figure 7a and Figure 7b, respectively. In both datasets, GSB dominates the spectra between 515 and 560 nm. The ESA is very broad and can be observed everywhere in the visible region except for the dominant GSB region. The dominant ESA in B2P (Figure 7a and 7b) from 460 to 515 nm matches with the perylene triplet absorption (see SI, Figure S3 and S4).[10] The ESA band in the range between 560 and 800 nm arises from contributions of both BODIPY and perylene triplet states.[25] Upon addition of 50 μM perylene to B2P (5 μM), the differential absorption signatures at 425 and 455 nm increase in intensity (see

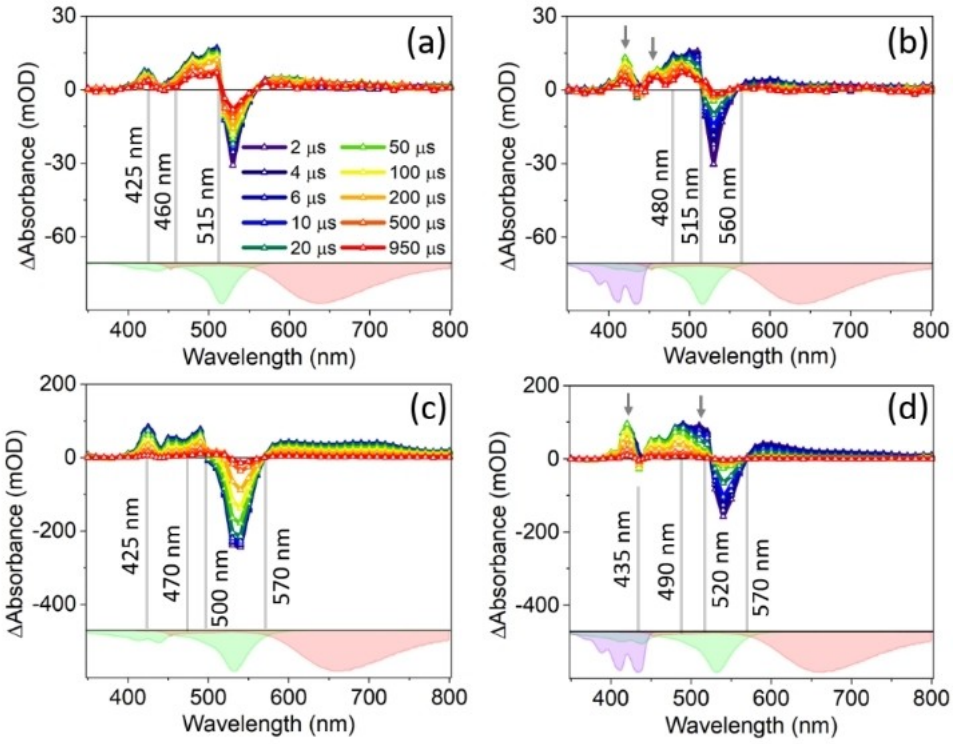

Figure 7. Nanosecond transient absorption spectra of (a) B2P – 5 μM, (b) B2P – 5 μM and perylene 50 μM, (c) B2PI – 5 μM, (d) B2PI – 5 μM and perylene 50 μM. In the bottom- inverted absorbance of photosensitizer is in green and inverted emission of photosensitizer is in red, inverted absorbance of perylene is in violet of the respective sample. Labels are consistent for all subfigures. Arrows in (b) and (d) show changes in the spectra with respect to (a) and (c), respectively, upon addition of 50 μM perylene. The excitation wavelength is 532 nm.

Figure 7b). We associate this with triplet-triplet energy transfer from BODIPY-dyads to the external perylene.[10,24]

Similarly, nanosecond transient absorption spectra of B2PI with and without the addition of perylene are shown in Figure 7c and 7d respectively. In B2PI (Figure 7c), GSB dominates between 500–570 nm. Outside this range, ESA dominates everywhere between 350 and 800 nm. Two ESA peaks are observed at 425 nm and 490 nm. Whereas, the addition of 50 μM of perylene (Figure 7d) increases the ESA at 425 nm and from 490 nm to 520 nm (see arrows). The GSB region shrinks and decreases in the 520–570 nm range due to the rise of ESA (superimposition) in 490–520 nm.

When comparing B2P and B2PI in Figure 7 (a and c), the negative GSB feature is red-shifted in B2PI which reflects the spectral shift already seen in the steady-state absorption spectra. The ESA (associated to triplet species) is much more intense in B2PI compared to B2P (under otherwise identical experimental conditions) due to the formation of a higher number of triplet species promoted by the presence of iodine (*vide supra*); for instance, ESA at 480 nm and 1 μs is 14 mOD and 58 mOD for B2P and B2PI, respectively. Furthermore, for B2P upon the addition of perylene, there is no rise in the ESA between 490–520 nm (see Figure 7a and b); however, for the B2PI sample, the ESA rise (490–520 nm) is significant upon the addition of perylene (see arrows in Figure 7c and d). This feature is attributed to TTET from triplet sensitizer to the external perylene, which increases the population of triplet perylene thus enhances ESA.

Due to the lack of complete orthogonality between the dyad pair (see Figure 4 and 5),[26] there will be a significant overlap of orbitals of the BODIPY and perylene moieties. Hence, the triplet states are expected to have common features of BODIPY and perylene. By the global fitting[50] of the kinetics of B2PI (1 μM and 5 μM), we observed three different species with three different characteristic lifetimes, as shown in Figure 8. Since, the BODIPY triplet ESA feature appears below 460 nm (see SI, Figure S3 and S4),[10] the decay associated spectra (DAS) associated with τ_2 is assigned to the decay of a BODIPY-centered state (T_2), the ESA of this spectra is also until *ca.* 460 nm (see Figure 8). The DAS associated with τ_1 is assigned to the decay of a perylene-centered state (T_1), the ESA of this spectra is until *ca.* 540 nm matching with ESA of triplet perylene (see SI, Figure S3 and S4).[10] The DAS with time constant τ_3 is assigned to the decay of the ^{3}CT state.

When the B2PI concentration (Figure 8) is increased from 1 μM to 5 μM, the BODIPY-centered triplet state lifetime reduces from 525 μs to 155 μs, the perylene-centered triplet state lifetime reduces from 1.5 ms to 560 μs, the reduction in lifetime occurs due to triplet-triplet annihilation. In further reducing the concentration of B2PI to 0.25 μM, the signal-to-noise ratio was very poor and a good fit could not be obtained. Hence, the lifetimes 60 μs, 525 μs, 1.5 ms obtained from 1 μM concentration are considered to be the intrinsic lifetimes of the three ^{3}CT, BODIPY-centered and perylene-centered states with negligible contribution from lifetime-reduction due to intermolecular annihilation, see SI Figure S6 for kinetics and fits.

The global fit of the B2P kinetics also shows three components with time-constants of 80 μs, 900 μs, and 2.5 ms assigned to the decay time-constants of ^{3}CT, BODIPY-centered, perylene-centered states (see SI, Figure S7); however, due to the lower triplet ESA the signal-to-noise is poor and lifetime values have a large margin of error of 20%. These lifetimes are still much higher than in case of the iodo-BODIPY triplet lifetime ($\tau = 62$ μs).[15,53] The B2P molecule at 12 μM is measured, which shows a fair signal (see SI, Figure S8).

Upon addition of external perylene to B2P and B2PI solution, TTET occurs, which lowers the triplet lifetime of the sensitizer.[28] For instance, when 50 μM of perylene is added to 5 μM of B2PI, the lifetimes of the sample are 11 μs, 107 μs and 512 μs (see SI, Figure S5 and S6). The three lifetimes are quenched lifetimes of the decay of ^{3}CT (11 μs), BODIPY-centered triplet (107 μs) and perylene-centered triplet (512 μs). Similar observations are made for B2P (5 μM; see Figure S7 and S10). The bimolecular energy transfer rate (k_{TTET}) is obtained using the Stern-Volmer plot depicted in Figure S12, k_{TTET} values for TTAUC systems containing B2P and B2PI are $(7.6 \pm 0.6) \cdot 10^8\ M^{-1} s^{-1}$ and $(8.3 \pm 0.5) \cdot 10^8\ M^{-1} s^{-1}$, respectively. Both systems have k_{TTET} values within the error range of each other; therefore, the rate-constant is considered equal ($\sim 8 \cdot 10^8\ M^{-1} s^{-1}$) for both systems, see SI for details. The time-resolved emission for B2P and B2PI with perylene at 470 nm is shown in SI Figure S11, the growing part of the emission reflects population of perylene triplet state

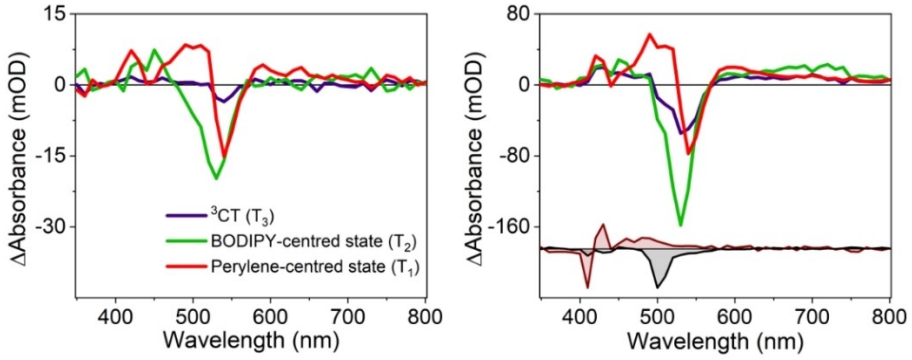

Figure 8. DAS of the global fit of the kinetics of (a) B2PI 1 μM, ^{3}CT- triplet charge transfer state (T_3), $\tau_3 = 60 \pm 6$ μs; BODIPY-centered state (T_2), $\tau_2 = 526 \pm 50$ μs; perylene-centered state (T_1), $\tau_1 = 1500 \pm 150$ μs (b) B2PI 5 μM, $\tau_3 = 66 \pm 7$ μs, $\tau_2 = 155 \pm 15$ μs, $\tau_1 = 560 \pm 50$ μs. In the bottom- two DAS components of the BODIPY 20 μM with perylene 50 μM (see SI, Figure S3 and S4). Labels are same for both sub figures.

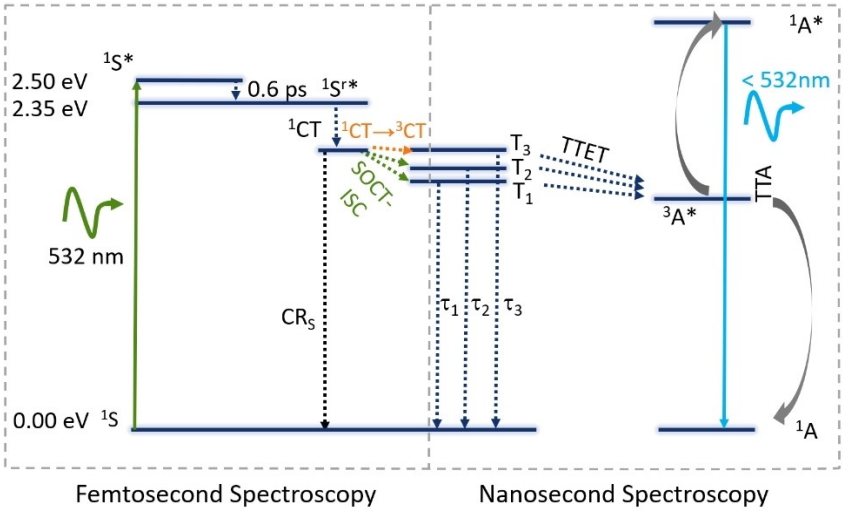

Figure 9. Model indicating processes from absorption of a 532 nm photon to emission of an anti-Stoke shifted blue photon. The SOCT-ISC time-constants for B2PI and B2P 662 ps, 1785 ps respectively. T_3 – triplet charge transfer state, T_2 – BODIPY-centered triplet, T_1 – perylene-centered triplet. The details of decay time-constants are given in Table 1. ^{1}S*: locally excited state and ^{1}S^r*: locally relaxed excited state, CR_S: charge recombination to ground state.

by TTET and the decay part of the curve reflects decay of perylene triplets by TTA.[18,54,55]

Conclusions

In summary, the photophysical properties of BODIPY-perylene dyads with and without an iodine substituent, in dioxane are studied using steady state, scalar-relativistic TDDFT simulations, femtosecond and nanosecond time-resolved studies. The TTA-UC is performed using perylene as annihilator with an anti-Stokes emission evident associated with perylene on excitation into the sensitizer. The femtosecond study reveals both the B2P and B2PI follow same pathways build-up of locally excited state and geometrical relaxation (~0.6 ps), charge separation and formation of charge transfer state (~4.5 ps), charge recombination to ground state (~280 ps) and charge recombination to triplet (685 ps for B2PI and 1785 ps for B2P), this confirms the triplet formation by charge recombination *i.e.* spin-orbit charge transfer intersystem crossing (SOCT-ISC), see Figure 9. We observe that iodine substitution enhances the SOCT-ISC as the triplet formation is visible by charge recombination. A significant contribution of ^{1}CT→^{3}CT population transfer by spin-orbit coupling is also observed. Nanosecond time-scale studies were performed to investigate the triplet lifetimes. For B2PI three distinct lifetimes were observed, associated with triplet charge transfer state- ^{3}CT (60 μs), BODIPY-centered triplet (525 μs) and perylene-centered triplet (1500 μs). Similarly, for B2P molecule, ^{3}CT (80 μs), BODIPY-centered triplet (900 μs) and perylene-centered triplet (2500 μs) states were observed. Upon addition of external perylene to the sensitizer solution, the triplet lifetimes are reduced which confirms quenching by triplet-triplet energy transfer and triplet-triplet annihilation processes. This study provides detailed new insights into photophysical properties of the triplet species when dyad molecules are non-orthogonal that should support further design and development of metal free dyad sensitizers for TTAUC and indeed other triplet state sensitizers.

Supporting information

Additional references cited within the Supporting information.[3,10,11,28,56]

Acknowledgements

All authors acknowledge the funding from the European Union's Horizon 2020 research and innovation programme under the Marie Skłodowska-Curie grant agreement No 813920 for LogicLab ITN. The calculations were performed at the Wrocław Centre for Networking and Supercomputing (grant No. 384) and at the Academic Computer Centre TASK in Gdańsk. KKJ gratefully acknowledge the support by Dr. Jens Uhlig for supporting with KimoPack. TEK, AP and NKS also gratefully acknowledge Science Foundation Ireland for funding under grants 19/FFP/6428 and 12/RC/2276_P2. Open Access funding enabled and organized by Projekt DEAL.

Conflict of Interests

There are no conflicts to declare.

Data Availability Statement

The data that support the findings of this study are available from the corresponding author upon reasonable request.

Keywords: BODIPY-perylene dyads · intersystem crossing · SOCT-ISC · spin orbit coupling · triplet-triplet annihilation upconversion (TTAUC)

[1] A. C. Benniston, G. Copley, *Phys. Chem. Chem. Phys.* **2009**, *11*, 4124–4131.
[2] M. A. Filatov, *Org. Biomol. Chem.* **2019**, *18*, 10–27.
[3] J. T. Ly, K. F. Presley, T. M. Cooper, L. A. Baldwin, M. J. Dalton, T. A. Grusenmeyer, *Phys. Chem. Chem. Phys.* **2021**, *23*, 12033–12044.
[4] K. Chen, Y. Dong, X. Zhao, M. Imran, G. Tang, J. Zhao, Q. Liu, *Front. Chem.* **2019**, *7*, 1–14.
[5] Y. Ni, J. Wu, *Org. Biomol. Chem.* **2014**, *12*, 3774–3791.
[6] D. O'Connor, A. Byrne, T. E. Keyes, *RSC Adv.* **2019**, *9*, 22805–22816.
[7] W. Zhang, A. Ahmed, H. Cong, S. Wang, Y. Shen, B. Yu, *Dyes and Pigment.* **2021**, *185*, 108937.
[8] A. Turksoy, D. Yildiz, E. U. Akkaya, *Coord. Chem. Rev.* **2019**, *379*, 47–64.
[9] Y. Çakmak, S. Kolemen, M. Buyuktemiz, Y. Dede, S. Erten-Ela, *New J. Chem.* **2015**, *39*, 4086–4092.
[10] M. Sittig, B. Schmidt, H. Görls, T. Bocklitz, M. Wächtler, S. Zechel, M. D. Hager, B. Dietzek, *Phys. Chem. Chem. Phys.* **2020**, *22*, 4072–4079.
[11] M. O. S. M. A. Filatov, S. Karuthedath, P. M. Polestshuk, S. Callaghan, K. J. Flanagan, T. Wiesner, F. Laquai, *ChemPhotoChem* **2018**, *2*, 606–615.
[12] J. Zhao, W. Wu, J. Sun, S. Guo, *Chem. Soc. Rev.* **2013**, *42*, 5323.
[13] K. Fujimoto, K. Kawai, S. Masuda, T. Mori, T. Aizawa, T. Inuzuka, T. Karatsu, M. Sakamoto, S. Yagai, T. Sengoku, M. Takahashi, H. Yoda, *Langmuir* **2019**, *35*, 9740–9746.
[14] A. Kamkaew, S. H. Lim, H. B. Lee, L. V. Kiew, L. Y. Chung, K. Burgess, *Chem. Soc. Rev.* **2013**, *42*, 77–88.
[15] Z. Wang, M. Ivanov, Y. Gao, L. Bussotti, P. Foggi, H. Zhang, N. Russo, B. Dick, J. Zhao, M. Di Donato, G. Mazzone, L. Luo, M. Fedin, *Chem. Eur. J.* **2020**, *26*, 1091–1102.
[16] X. Cui, A. M. El-Zohry, Z. Wang, J. Zhao, O. F. Mohammed, *J. Phys. Chem. C* **2017**, *121*, 16182–16192.
[17] W. Wu, H. Guo, W. Wu, S. Ji, J. Zhao, *J. Org. Chem.* **2011**, *76*, 7056–7064.
[18] Z. Wang, A. A. Sukhanov, A. Toffoletti, F. Sadiq, J. Zhao, A. Barbon, V. K. Voronkova, B. Dick, *J. Phys. Chem. C* **2019**, *123*, 265–274.
[19] K. Chen, W. Yang, Z. Wang, A. Iagatti, L. Bussotti, P. Foggi, W. Ji, J. Zhao, M. Di Donato, *J. Phys. Chem. A* **2017**, *121*, 7550–7564.
[20] Z. Wang, J. Zhao, *Org. Lett.* **2017**, *19*, 4492–4495.
[21] K. Chen, W. Yang, Z. Wang, A. Iagatti, L. Bussotti, P. Foggi, W. Ji, J. Zhao, M. Di Donato, *J. Phys. Chem. A* **2017**, *121*, 7550–7564.
[22] D. J. Gibbons, A. Farawar, P. Mazzella, S. Leroy-Lhez, R. M. Williams, *Photochem. Photobiol. Sci.* **2020**, *19*, 136–158.
[23] S. Suzuki, M. Kozaki, K. Nozaki, K. Okada, *J. Photochem. Photobiol. C* **2011**, *12*, 269–292.
[24] J. T. Buck, A. M. Boudreau, A. DeCarmine, R. W. Wilson, J. Hampsey, T. Mani, *Chem* **2019**, *5*, 138–155.
[25] J. T. Buck, M. Andrew, R. W. Wilson, J. T. Buck, A. M. Boudreau, R. W. Wilson, J. Hampsey, *Chem* **2018**, *5*, 138–155.
[26] R. A. Arellano-Reyes, A. Prabhakaran, R. C. E. Sia, J. Guthmuller, K. K. Jha, T. Yang, B. Dietzek-Ivanšić, V. McKee, T. E. Keyes, *Chem. Eur. J.* **2023**, *29*, e202300239.
[27] T. Yang, R. A. Arellano-Reyes, R. C. Curley, K. K. Jha, A. Chettri, T. E. Keyes, B. Dietzek-Ivanšić, *Chem. Eur. J.* **2023**, *29*, e202300224.
[28] K. K. Jha, A. Prabhakaran, C. S. Burke, M. Schulze, U. S. Schubert, T. E. Keyes, M. Jäger, B. D. Ivanšić, *J. Phys. Chem. C* **2022**, *126*, 4057–4066.
[29] C. A. Parker, C. G. Hatchard, C. A. Parker, C. G. Hatchard, *Proc. R. Soc. Lond. A Math. Phys. Sci.* **1962**, *269*, 574–584.
[30] V. Gray, K. Moth-Poulsen, B. Albinsson, M. Abrahamsson, *Coord. Chem. Rev.* **2018**, *362*, 54–71.
[31] T. N. Singh-Rachford, F. N. Castellano, *Coord. Chem. Rev.* **2010**, *254*, 2560–2573.
[32] Y. Lei, K. Chen, G. Tang, J. Zhao, G. G. Gurzadyan, *J. Photochem. Photobiol. A* **2020**, *398*, 112573.
[33] R. Siebert, D. Akimov, M. Schmitt, A. Winter, U. S. Schubert, B. Dietzek, J. Popp, *ChemPhysChem* **2009**, *10*, 910–919.
[34] A. Chettri, J. H. Kruse, K. Kumar Jha, L. Dröge, I. Romanenko, C. Neumann, S. Kupfer, A. Turchanin, S. Rau, F. H. Schacher, B. Dietzek, *Chem. Eur. J.* **2021**, *27*, 17049–17058.
[35] L. Dura, M. Wächtler, S. Kupfer, J. Kübel, J. Ahrens, S. Höfler, M. Bröring, B. Dietzek, T. Beweries, *Inorganics* **2017**, *5*, 21.
[36] M. J. Frisch, G. W. Trucks, H. B. Schlegel, G. E. Scuseria, M. A. Robb, J. R. Cheeseman, G. Scalmani, V. Barone, G. A. Petersson, H. Nakatsuji, *Gaussian 16, Revision C.01* **2016**.
[37] F. Neese, F. Wennmohs, U. Becker, C. Riplinger, *J. Chem. Phys.* **2020**, *152*, 224108.
[38] S. Y. Haoyu, X. He, S. L. Li, D. G. Truhlar, *Chem. Sci.* **2016**, *7*, 5032–5051.
[39] F. Weigend, R. Ahlrichs, *Phys. Chem. Chem. Phys.* **2005**, *7*, 3297–3305.
[40] F. Weigend, *Phys. Chem. Chem. Phys.* **2006**, *8*, 1057–1065.
[41] S. Grimme, S. Ehrlich, L. Goerigk, *J. Comput. Chem.* **2011**, *32*, 1456–1465.
[42] S. Grimme, *Wiley Interdiscip. Rev.: Comput. Mol. Sci.* **2011**, *1*, 211–228.
[43] L. Goerigk, A. Hansen, C. Bauer, S. Ehrlich, A. Najibi, S. Grimme, *Phys. Chem. Chem. Phys.* **2017**, *19*, 32184–32215.
[44] J. Tomasi, B. Mennucci, R. Cammi, *Chem. Rev.* **2005**, *105*, 2999–3094.
[45] A. V Marenich, C. J. Cramer, D. G. Truhlar, *J. Phys. Chem. B* **2009**, *113*, 6378–6396.
[46] J. T. Ly, K. F. Presley, T. M. Cooper, L. A. Baldwin, M. J. Dalton, T. A. Grusenmeyer, *Phys. Chem. Chem. Phys.* **2021**, *23*, 12033–12044.
[47] Y. Tian, Q. Cheng, H. Dang, H. Qian, C. Teng, K. Xie, L. Yan, *Dyes and Pigment.* **2021**, *194*, 109611.
[48] Q. Zhou, M. Zhou, Y. Wei, X. Zhou, S. Liu, S. Zhang, B. Zhang, *Phys. Chem. Chem. Phys.* **2017**, *19*, 1516–1525.
[49] E. Bassan, A. Gualandi, P. G. Cozzi, P. Ceroni, *Chem. Sci.* **2021**, *12*, 6607–6628.
[50] C. Müller, T. Pascher, A. Eriksson, P. Chabera, J. Uhlig, *J. Phys. Chem. A* **2022**, *126*, 4087–4099.
[51] Z. Wei, A. M. Philip, W. F. Jager, F. C. Grozema, *J. Phys. Chem. C* **2022**, *126*, 19250–19261.
[52] Y. Hou, X. Zhang, K. Chen, D. Liu, Z. Wang, Q. Liu, J. Zhao, A. Barbon, *J. Mater. Chem. C Mater* **2019**, *7*, 12048–12074.
[53] Y. Hou, J. Liu, N. Zhang, J. Zhao, *J. Phys. Chem. A* **2020**, *124*, 9360–9375.
[54] Y. Zhao, R. Duan, J. Zhao, C. Li, *Chem. Commun.* **2018**, *54*, 12329–12332.
[55] A. C. Benniston, A. Harriman, I. Llarena, C. A. Sams, *Chem. Mater.* **2007**, *19*, 1931–1938.
[56] A. Olesund, V. Gray, J. Mårtensson, B. Albinsson, *J. Am. Chem. Soc.* **2021**, *143*, 5745–5754.

Manuscript received: April 11, 2023
Revised manuscript received: June 9, 2023
Accepted manuscript online: June 9, 2023
Version of record online: July 24, 2023